


Article

Crystallographic Orientation Dependence of Nitrogen Mass Transport in Austenitic Stainless Steel

Teresa Moskalioviene and Arvidas Galdikas * 

Physics Department, Kaunas University of Technology, Studentu 50, LT-51368 Kaunas, Lithuania; teresa.moskalioviene@ktu.lt

* Correspondence: arvidas.galdikas@ktu.lt; Tel.: +370-600-48-897

Received: 10 April 2020; Accepted: 7 May 2020; Published: 9 May 2020



Abstract: The lattice stress-induced diffusion of nitrogen and hydrogen in austenitic stainless steel, taking place during nitriding in nitrogen/hydrogen plasma, is analyzed in the presented work. Stress-induced diffusion has an anisotropic nature and depends on the orientation of the crystal lattice. However, during simulations, it is not enough to take into account only the anisotropy of stress-induced diffusion, since this leads to contradictory results when comparing with experimental data. The problem is the surface concentration of nitrogen. Processes on the steel surface such as adsorption, desorption and heterogeneous chemical reactions are also very important. In the presented work, it is shown that these surface processes also have anisotropic natures, and it is very important to take this anisotropy into account during simulations. The influence of anisotropic surface processes on austenitic steel nitriding is analyzed in this study. It is shown that the nitrogen diffusion is anisotropic due to the effects of the anisotropic stress gradient and the anisotropic effects on the steel surface.

Keywords: nitriding; expanded austenite; anisotropic elasticity; stress-assisted anisotropic diffusion; modeling

1. Introduction

Austenitic stainless steels (ASS) are often used as engineering materials in many industrial applications among which are food and chemical processing, the automotive industry, and some surgical implants due to very high corrosion resistance in many aggressive environments because of a passive Cr_2O_3 surface film. Whereas the corrosion resistance of these materials is excellent, their hardness (with a surface hardness of $\sim 200\text{--}300$ HV) and wear resistance are relatively low. Many attempts have therefore been made to increase the wear resistance without deteriorating the corrosion resistance. Plasma nitriding is one of the well-known processes for the surface modification of metals and alloys. Thus, this technology is rapidly gaining acceptance for the treatment of ASSs in various industry sectors to achieve combined improvements in wear and corrosion resistance.

The low-temperature plasma nitriding (performed at temperatures up to 450 °C) of ASS results in improved properties, such as a greatly increased surface hardness, wear resistance, fatigue resistance, and corrosion resistance [1–13]. Such a hardening process is related to the lattice distortion of the fcc austenitic phase (γ phase), leading to the formation of nitrogen-rich expanded austenite (γ_{N} phase), with a hardness close to 1500 HV and no loss of corrosion resistance [6,14]. The high nitrogen content dissolved in the γ_{N} crystalline lattice leads to a noticeable expansion of the lattice, giving rise to high compressive residual stresses [9–12]. Intensive studies on γ_{N} phase structure and formation have been undertaken by various researchers in the past several decades, and a comprehensive review of the scientific literature regarding the formation, characteristics and properties of the γ_{N} phase is presented

in [15]. However, despite the numerous investigations, the structure and formation of this phase have not yet been completely clarified.

One such phenomenon is that the lattice parameter expansion caused by interstitial nitrogen is crystallographically anisotropic. Typically, the lattice parameter a_{hkl} , determined from the d-spacing of the (200) plane, is greater than that determined from the d-spacing of the (111), (220), (311) or (222) planes [6,8,16–19]. Furthermore, the surface nitrogen content and the thickness of the case of the expanded austenite were shown to depend on the crystal orientation, i.e., an increase in the order (100) > (110) > (111) for different crystallographic orientations [6,8,16–19]. A recent explanation for this phenomenon involves the formation of stacking faults and high compressive residual stresses in the nitrated layer resulting in a highly distorted and disordered fcc structure [15]. Such a difference in diffusion depth during expanded austenite formation was explained by the authors in [20] by stress anisotropy, which gave rise to an orientation dependence of the activation energy for diffusion due to the activation volume for diffusion [20]. Moreover, the effect of anisotropic lattice expansion could be explained by the residual compressive stress developed during nitriding, which varies as a function of the crystallographic orientation of the ASS specimen due to the elastically anisotropic nature of austenite [11,21,22]. As mentioned in our previous studies [23–27], the stress induced by the concentration gradient of interstitials inside a solid affects the transport of nitrogen. Thus, an elastic field is capable of creating an additional component of the driving force for the nitrogen transport. A straightforward interpretation of strains in terms of stresses can be obstructed if the single crystallites composing the specimen are elastically anisotropic. A so-called grain interaction model is needed to describe the distribution of stresses and strains over the crystallographically differently oriented crystallites in the specimen. In our case, for the calculation of the mechanical elastic constants of bulk polycrystals from single-crystal elastic compliances, we use the Reuss grain-interaction model, i.e., the stress tensor for each crystallite is assumed to be equal to the mechanical stress tensor [28]. By taking to account the Reuss grain-interaction model [28] and elastic anisotropy of ASS [21,22], it may be considered that the induced internal stress is strongly dependent on the crystallographic orientation and, again, influences nitrogen diffusion. As a consequence, the nitrogen penetration depth also depends on the crystallographic orientation of ASS sample. Furthermore, the process of nitriding is influenced not only by the volumetric processes but also by processes on the surface. The rate of the nitriding reaction between a nitriding medium and a solid substrate mainly depends on surface anisotropy, i.e., the anisotropic surface energy. As a result, the nitrogen fluxes passing through the surface of different crystallographic orientations can be different.

Against the above background, this work aims to study the impacts of the elastic anisotropy of ASS, as well as the anisotropy of the surface free energies, on the phenomenon of anisotropic nitrogen penetration during low temperature plasma nitriding. In this paper, the anisotropy of surface processes such as adsorption and heterogeneous chemical reactions is incorporated into the model, which was not previously done. This aspect is important, and it is shown that if the anisotropic nature of adsorption and surface chemical reactions is not taken into account, the results contradict experimental observations, considering the kinetics of nitrogen surface concentration.

2. Mass Transport Model

A generalized formalism of the stress-assisted diffusion model presented in our previous work [23–27] is presented hereafter, allowing both the isotropic and anisotropic nitriding of ASS to be simulated. Based on Fick's law the interstitial atom (nitrogen and/or hydrogen) diffusion through the austenite phase can be described as:

$$\frac{\partial C_{\text{int}}}{\partial t} + \nabla \cdot \vec{J}_{\text{int}} = 0 \quad (1)$$

where C_{int} is the interstitial concentration and J_{int} is the interstitial atom flux. In the case of the interstitial atom's diffusion into the austenite phase, the flux of this species can be written as [29,30]:

$$\vec{J}_{\text{int}} = -L_{\text{int}} \nabla \mu_{\text{int}}(C_{\text{int}}, \sigma) \quad (2)$$

where L_{int} is the Onsager coefficient and $\mu_{\text{int}}(C_{\text{int}}, \sigma)$ is the chemical potential of interstitials in a metallic lattice, which at constant temperature depends on the interstitial concentration C_{int} (symbolizes the relative concentration of interstitials in a metallic lattice) and stress σ . In general, the gradient of the chemical potential is the main driving force for interstitial atom diffusion in the metallic lattice. The stress effects on the interstitial's diffusion are reflected in the chemical potential, which incorporates chemical and mechanical energies. For a system under a stress σ , the chemical potential of interstitial atoms in lattice sites is given by [29,30]:

$$\mu_{\text{int}}(C_{\text{int}}, \sigma) = \mu_{\text{int}}^0 + RT \ln(f_{\text{int}} \cdot C_{\text{int}}) - V_{\text{int}} \sigma \quad (3)$$

where $V_{\text{int}} \sigma$ is the stress-dependent part of chemical potential; $(\mu_{\text{int}}^0 + RT \ln(f_{\text{int}} \cdot C_{\text{int}}))$ denotes the chemical potential of interstitial atoms in the stress-free state ($\sigma = 0$); μ_{int}^0 is the standard chemical potential; f_{int} is the activity coefficient; V_{int} is the partial molar volume of interstitials in the solid matrix; and R and T are the universal gas constant and the absolute temperature, respectively.

Thus, a phenomenological consideration of the hydrostatic stress' effects on interstitial behavior in metals yields the equation of stress-assisted diffusion under isothermal conditions (and by assuming an ideal solid solution so that $\frac{\partial \ln(f_{\text{int}})}{\partial \ln(C_{\text{int}})} = 0$) as follows [24,27,29,30]:

$$\vec{J}_{\text{int}} = -L_{\text{int}} \nabla \mu_{\text{int}} = -\frac{L_{\text{int}} RT}{C_{\text{int}}} \nabla C_{\text{int}} + L_{\text{int}} V_{\text{int}} \nabla \sigma \quad (4)$$

where $\frac{L_{\text{int}} RT}{C_{\text{int}}} = D_{\text{int}}$ is (in m^2/s) is the diffusion coefficient of interstitial atoms in a stress-free solid.

Substituting Equation (4) into Equation (1), the diffusion equation including the coupling effect of stresses and diffusion is obtained by:

$$\frac{\partial C_{\text{int}}}{\partial t} = -\nabla \cdot \vec{J}_{\text{int}} = -\nabla \cdot \left(-D_{\text{int}} \nabla C_{\text{int}} + \frac{D_{\text{int}} \cdot C_{\text{int}} \cdot V_{\text{int}}}{RT} \nabla \sigma \right) \quad (5)$$

To evaluate the compressive stress and the compositional strain induced by the interstitial atom diffusion in the expanded austenite, a mechanical model recently developed in our previous work [26] was used. The dependence of compositionally induced biaxial compressive residual stresses in the $[h k l]$ direction on the concentration of interstitials is obtained by [26,31,32]:

$$\sigma(hkl) = \frac{1}{\left(S_{11} - 2 \cdot_{hkl} \cdot \left(S_{11} - S_{12} - \frac{1}{2} S_{44} \right) \right)} \cdot \frac{\beta_{\text{int}}}{a_0} \cdot C_{\text{int}} = -X_{\text{stress}(hkl)} \cdot C_{\text{int}} \quad (6)$$

The anisotropic stress factor $X_{\text{stress}(hkl)}$ in any crystallographic direction $[h k l]$ depends on the so-called orientation factor $P_{hkl} = \left(h^2 \cdot k^2 + h^2 \cdot l^2 + k^2 \cdot l^2 \right) \cdot \left(h^2 + k^2 + l^2 \right)^{-2}$ [31] and on the Young's modulus $E_{hkl} = \left(S_{11} - 2 \cdot_{hkl} \cdot \left(S_{11} - S_{12} - \frac{1}{2} S_{44} \right) \right)^{-1}$, where h, k and l are Miller indexes; and S_{11}, S_{12} and S_{44} are independent intrinsic single crystal elastic constants (elastic compliances), which are related to the non-zero stiffness tensor components C_{ij} by the relationships: $S_{11} = \frac{(C_{11} + C_{12})}{(C_{11} - C_{12})(C_{11} + 2C_{12})}$, $S_{12} = \frac{-C_{12}}{(C_{11} - C_{12})(C_{11} + 2C_{12})}$ and $S_{44} = \frac{1}{C_{44}}$. In addition, a linear relationship exists between the total strain in the $[h k l]$ direction (which is linearly related to the stress through Hooke's law, i.e., $\varepsilon(hkl) = \frac{1}{E_{hkl}} \cdot \sigma(hkl)$) and the mean concentration of interstitials in the expanded austenite, i.e., $\varepsilon(hkl) = \frac{\beta_{\text{int}}}{a_0} \cdot C_{\text{int}}$ [26], where β_{int} is the Vegard's constant for interstitial atoms dissolved in austenite and a_0 is the lattice parameter of the austenite (strain-free). It is important to note that for nitrated layers containing the γ_{N} phase, various types of strain (thermal, compositional, elastic and plastic) can be considered. However, we only take into account anisotropic compositional strain in our model. Hence, the incorporation of the

compositional, thermal, plastic and elastic contributions to the strain, induced in the austenite lattice due to the formation of the γ_N phase, is the main goal for our future investigations.

Introducing Equation (6) into Equation (5) as the diffusion is one-dimensional along the x -direction (the x axis is the diffusion axis), the diffusion governing equation considering the effect of stress-assisted anisotropic diffusion takes the following form:

$$\frac{\partial C_{\text{int}}(x, t)}{\partial t} = \Phi_{0\text{int-hkl}}(0, t) + \nabla_x \left(D_{\text{int}} \left(1 + \frac{V_{\text{int}} C_{\text{int}}(x, t)}{RT} \cdot X_{\text{stress}(hkl)} \right) \nabla_x C_{\text{int}}(x, t) \right) \quad (7)$$

where ∇_x is x -axis projection of the gradient and $\Phi_{0\text{int-hkl}}$ is the adsorption term, which describes the process of interstitial atom adsorption on the steel surface (i.e. $\Phi_{0\text{int}}(x \neq 0, t) = 0$ and $\Phi_{0\text{int}}(x = 0, t) \neq 0$).

The process of nitriding is influenced not only by the processes in the bulk but also by processes on the surface. Experimental studies in [33–35] and our earlier theoretical studies [25,36] have shown that hydrogen has an important role in the nitriding process. A detailed description of the kinetic model of nitrogen and hydrogen adsorption in ASS taking place during plasma nitriding is proposed in our previous work [25]. The processes of adsorption, desorption, and surface reactions occurring on the steel surface during interaction with N_2 – H_2 plasma were represented by the following steps: (1) the adsorption and dissociation of nitrogen and hydrogen molecules, (2) the formation of water molecules and desorption (oxygen chemical etching by hydrogen), (3) the adsorption, dissociation and desorption of oxygen from residual gas during the nitriding process, (4) the adsorption and dissociation of NH radicals formed in the N_2 – H_2 mixture, and (5) the diffusion of nitrogen and hydrogen into the bulk of steel. Furthermore, it is well known that adsorption, desorption and surface reactions depend on surface energy. According to the thermodynamic theories of crystal growth [37,38], the surface energy is generally dependent on the orientation of the surface, i.e., anisotropy of the surface energy leads to anisotropy of the adsorption term $\Phi_{0\text{int-hkl}}$ in Equation (7). For fcc metals, as predicted by a bond-breaking model for the surface energies of solids in work [39] and by the embedded-atom method in [40], the close-packed (111) surface has the lowest surface energy. The surface energies for the other surface orientations increase linearly with an increasing angle between the surfaces (hkl) and (111). Thus, based on the principle of surface energy minimization, the adsorption/desorption probabilities and surface reactions rates on the (111) surface have the lowest values. The anisotropy of the surface free energies is exactly described in terms of the Miller indices in [39] (see [39], Table 4). It was shown that surface free energy of fcc crystals is directly proportional to $(h^2 + k^2 + l^2)^{-1/2}$ and consistently supports the trend $\gamma(111) < \gamma(110) < \gamma(100)$. Thus, the developed model equations (see Equation (1) in [25]) for the adsorption, desorption and chemical surface reactions of nitrogen and hydrogen were modified by including the crystal orientation factor $A_{hkl} = (h^2 + k^2 + l^2)^{-1/2}$:

For a steel surface layer ($x = 0$):

$$\left\{ \begin{array}{l} \frac{dC_{H_2}}{dt} = A_{hkl} \left(\alpha_H \cdot i_{H_2} \cdot (C_{Fe}^{(x)} + C_O^{(x)}) - dis_{H_2} \cdot C_{H_2} + \frac{1}{2} \cdot R_{NH} \cdot C_{NH} \cdot C_H^{(x)} - des_{H_2} \cdot C_{H_2} \right) \\ \frac{dC_{NH}}{dt} = A_{hkl} \left(\alpha_{NH} \cdot i_{NH} \cdot (C_H^{(x)} + C_{Fe}^{(x)}) - R_{NH} \cdot C_{NH} \cdot C_H^{(x)} \right) \\ \frac{dC_{O_2}}{dt} = A_{hkl} \left(\alpha_O \cdot i_{O_2} \cdot C_{Fe}^{(x)} - dis_{O_2} \cdot C_{O_2} - des_{O_2} \cdot C_{O_2} \right) \\ \frac{dC_O^{(x)}}{dt} = A_{hkl} \left(2 \cdot dis_{O_2} \cdot C_{O_2} - \alpha_H \cdot i_{H_2} \cdot C_O^{(x)} - \frac{1}{2} \cdot R_{H_2O} \cdot C_O^{(x)} \cdot (C_H^{(k)})^2 \right) + \frac{D_O}{h^2} \cdot (C_O^{(x+1)} - C_O^{(x)}) \\ \frac{dC_{N_2}}{dt} = A_{hkl} \left(\alpha_N \cdot i_{N_2} \cdot C_{Fe}^{(x)} - dis_{N_2} \cdot C_{N_2} \right) \\ \frac{dC_{Fe}^{(x)}}{dt} = A_{hkl} \left(-2 \cdot dis_{O_2} \cdot C_{O_2} + des_{H_2} \cdot C_{H_2} + des_{O_2} \cdot C_{O_2} + R_{H_2O} \cdot C_O^{(x)} \cdot (C_H^{(x)})^2 - \right. \\ \left. - \alpha_O \cdot i_{O_2} \cdot C_{Fe}^{(x)} - \alpha_H \cdot i_{H_2} \cdot C_{Fe}^{(x)} - \alpha_{NH} \cdot i_{NH} \cdot C_{Fe}^{(x)} - \alpha_N \cdot i_{N_2} \cdot C_{Fe}^{(x)} \right) + \frac{D_{Fe}}{h^2} \cdot (C_{Fe}^{(x+1)} - C_{Fe}^{(x)}) \\ \Phi_{0H-hkl} = \frac{dC_H^{(x)}}{dt} = A_{hkl} \left(2 \cdot dis_{H_2} \cdot C_{H_2} - \frac{1}{2} \cdot R_{H_2O} \cdot C_O \cdot (C_H^{(x)})^2 - \alpha_{NH} \cdot i_{NH} \cdot C_H^{(x)} \right) \\ \Phi_{0N-hkl} = \frac{dC_N^{(x)}}{dt} = A_{hkl} \left(2 \cdot dis_{N_2} \cdot C_{N_2} + \frac{1}{2} \cdot R_{NH} \cdot C_{NH} \cdot C_H^{(x)} \right) \end{array} \right. \quad (8)$$

where C_{H_2} , C_H , C_{NH} , C_{O_2} , C_O , C_{N_2} , C_{Fe} and C_N are the relative concentrations of H_2 , H , NH , O_2 , O , N_2 , Fe and N respectively; α_{NH} , α_O , α_H , and α_N are the sticking coefficients of the NH radical, O_2 , H_2 and N_2 , respectively, to the corresponding steel surface components (possible adsorption sites); i_k is the relative flux of the k -th component to the surface; R_{NH,H_2O} are the reaction rate constants; des_k and dis_k are the desorption and dissociation probabilities of the k -th component, respectively; h is the thickness of the layer; and D is diffusion coefficient.

The process of the plasma nitriding of ASS (due to interaction with N_2 – H_2 plasma) can be viewed as diffusion in a vapor-solid diffusion couple, as shown schematically in Figure 1.

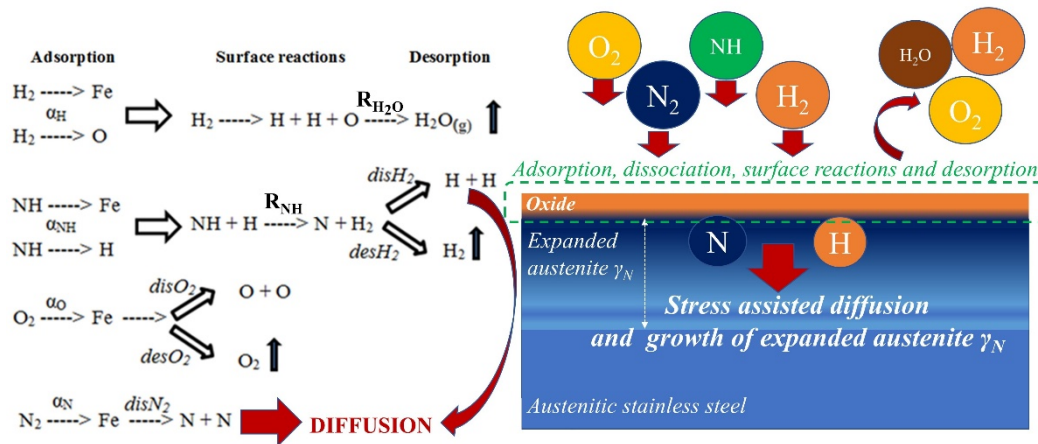


Figure 1. Schematic presentation of the elementary processes taking place during plasma nitriding.

3. Results and Discussion

This work aims to study the impacts of the elastic anisotropy of ASS, as well as the anisotropy of the surface free energies, on the phenomenon of anisotropic nitrogen penetration during low temperature nitriding. The governing equations (Equations (7) and (8)) were solved by a finite-difference method. The material properties of AISI 316L austenitic stainless steel and nitriding parameters used in the numerical simulation are listed in Table 1.

Table 1. Simulation parameters.

α_O	0.5	dis_{H_2}, s^{-1}	0.5	t, h	3
α_{NH}	0.1	dis_{N_2}, s^{-1}	0.9	$T, ^\circ C$	400
α_H	0.2	dis_{O_2}, s^{-1}	0.8	$V_N, m^3/mol$	3.9×10^{-5}
α_N	0.2	R_{NH}, s^{-1}	0.5	$V_H, m^3/mol$	1.6×10^{-5}
des_{O_2}, s^{-1}	0.2	R_{H_2O}, s^{-1}	0.5	For AISI 316L γ_N phase [41]	
des_{H_2}, s^{-1}	0.3	$D_O, cm^2 s^{-1}$	1×10^{-10}	C_{11}, GPa	307.2
i_{N_2}, s^{-1}	28.0×10^{-4}	$D_{Fe}, cm^2 s^{-1}$	1×10^{-14}	C_{12}, GPa	134.1
i_{O_2}, s^{-1}	1.9×10^{-6}	$D_{intN}, cm^2 s^{-1}$	8.2×10^{-13}	C_{44}, GPa	46.0
i_{H_2}, s^{-1}	12.0×10^{-6}	$D_{intH}, cm^2 s^{-1}$	16.4×10^{-13}	$X_{stressH}, MPa/at. \%$	$X_{stressN}/3$ [36]
i_{NH}, s^{-1}	was calculated according to the procedure as in [25]			$X_{stressN}, MPa/at. \%$ (for No DIF _{hkl} model)	200 [36]

A key element of the presented stress-assisted diffusion model is the anisotropic stress factor, $X_{stress(hkl)}$, which depends on the crystallographic orientation-dependent elastic modulus of ASS. Recently, in our previous work [26], it was found that the stress anisotropy (taking to account the anisotropy in the Young's modulus for the fcc crystal) has a significant impact on the nitrogen

concentration evolution during the expanded austenite formation. As mentioned above, the anisotropic stress factor, $X_{stress(hkl)}$, depends on the orientation factor, P_{hkl} , and Young's modulus, E_{hkl} (see Equation (6)). Furthermore, $X_{stress(hkl)}$ is the greatest for (100), the smallest for (111) and has intermediate values for the other crystal orientations. In work [26], we have shown that the values of the nitrogen penetration depths correlate well with the values of the anisotropic stress factor, $X_{stress(hkl)}$, i.e., they are the lowest for (111), the deepest for (100) and intermediate for the other orientations. According to the experimental results in [6,8,16–19], it can be concluded that the nitrogen surface concentration also increases in the order (111) < (110) < (100) for different crystallographic orientations. However, as we have shown in [26], if not taking into account the anisotropic nature of the adsorption, desorption and surface reactions, the calculated results show the opposite trend, i.e., the surface nitrogen content increases in the order (100) < (110) < (111). Thus, the main reason for current study is to solve this discrepancy between the calculation results and experimental observations.

The solution of this problem was split into two aspects. Firstly, experimental studies in [33–35] and our earlier theoretical studies [25,36] have shown that hydrogen has an important role in the nitriding process. Thus, the effects of the hydrogen on the adsorption, desorption and surface reaction processes occurring on the ASS surface due to interaction with N_2-H_2 plasma, as well as the hydrogen stress-assisted diffusion processes into the bulk of steel, should be considered. Secondly, adsorption, desorption and surface reaction processes are expected to be greatly affected by the surface tension or surface energy. Generally, the crystalline nature of materials leads to the anisotropy of the physical quantities, such as surface energy or surface tension, which must be taken into account in theoretical studies. Thus, the anisotropy of adsorption term, $\Phi_{0\ int-hkl}$, in Equation (7) was described in terms of the Miller indices according to the predicted results for fcc metals in [39,40], where the relationship between the values of the surface energies of low index planes was summarized as $\gamma(111) < \gamma(110) < \gamma(100)$.

For sequential coupling analysis, both isotropic and anisotropic surface effects (due to interaction with N_2-H_2 plasma) were compared in a single analysis. In order to validate the effects of isotropic hydrogen and nitrogen adsorption, desorption and surface reaction processes on the nitrogen distribution resulting from low temperature plasma nitriding, the simulation was performed using a model based on Equations (7) and (8) with the anisotropic $X_{stress(hkl)}$ term but with the isotropic adsorption term $\Phi_{0\ int-hkl}$ (i.e., with $A_{hkl} = 1$ for all crystallographic orientations). The results are presented in Figure 2 in the 1.1–1.3 curves (for different orientation single crystals, No $ADS_{hkl} + DIF_{hkl}$ curves). It is found that the nitrogen penetration depth is highest for the (100) oriented crystal and smallest for the (111) oriented crystal and that the nitrogen penetration depth follows the order (100) > (110) > (111). The same order is shown for the experimentally measured nitrogen diffusion depths [6,8,16–19]. However, as is clearly seen in Figures 2 and 3 (square points, No $ADS_{hkl} + DIF_{hkl}$ model), the surface concentration of nitrogen shows an opposite tendency, i.e., the surface nitrogen content increases in the order (100) < (110) < (111), and these results are not consistent with the experimental observations. Hence, the evaluation of isotropic hydrogen/nitrogen adsorption, desorption and surface reaction processes on the ASS surface does not allow the results of calculations to coincide with the experimental observations. To illustrate the effects of anisotropic surface processes, additional simulation was performed using a model based on Equations (7) and (8) with the anisotropic $X_{stress(hkl)}$ term and with the anisotropic adsorption term $\Phi_{0\ int-hkl}$ (i.e., with different values of A_{hkl} for different crystallographic orientations). The nitrogen depth profiles in the (100), (110) and (111) oriented single crystals were calculated and are presented in Figure 2 (2.1–2.3 curves, $ADS_{hkl} + DIF_{hkl}$ model). For this case, the values of nitrogen penetration depth and surface concentration are given in Figure 3 (circular points, $ADS_{hkl} + DIF_{hkl}$ model). It is seen that the penetration depth and surface concentration follow the order (100) > (110) > (111), and this is in qualitative agreement with the experimental results. By comparing the results shown in Figures 2 and 3, it can be concluded that the nitrogen diffusion is anisotropic due to effects of the anisotropic stress gradient, nitrogen/hydrogen concentration gradient and anisotropic effects on the steel surface.

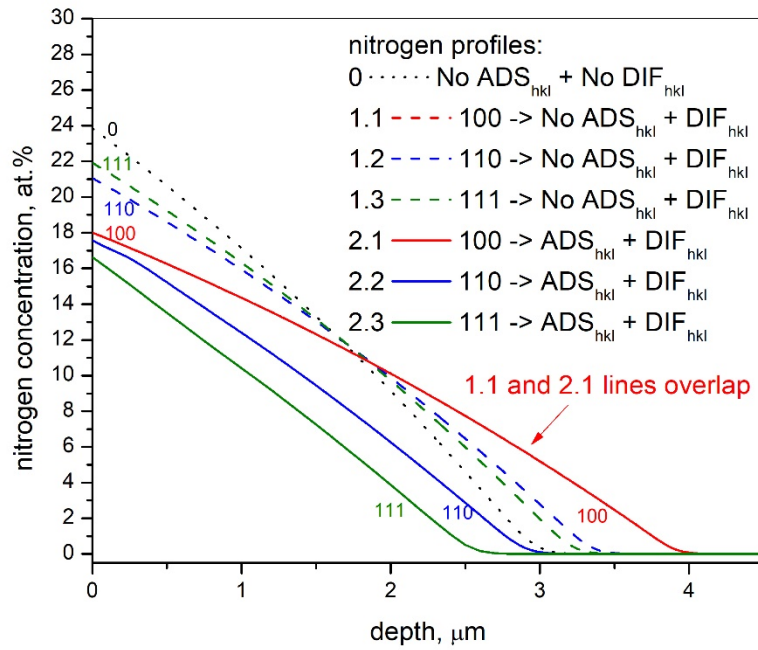


Figure 2. Depth profiles of nitrogen for different orientations of crystallites, calculated for three different cases: (0) isotropic surface processes and isotropic diffusion (No ADS_{hkl} + No DIF_{hkl}), (1) isotropic surface processes and anisotropic diffusion (No ADS_{hkl} + DIF_{hkl}), and (2) anisotropic surface processes and anisotropic diffusion (ADS_{hkl} + DIF_{hkl}).

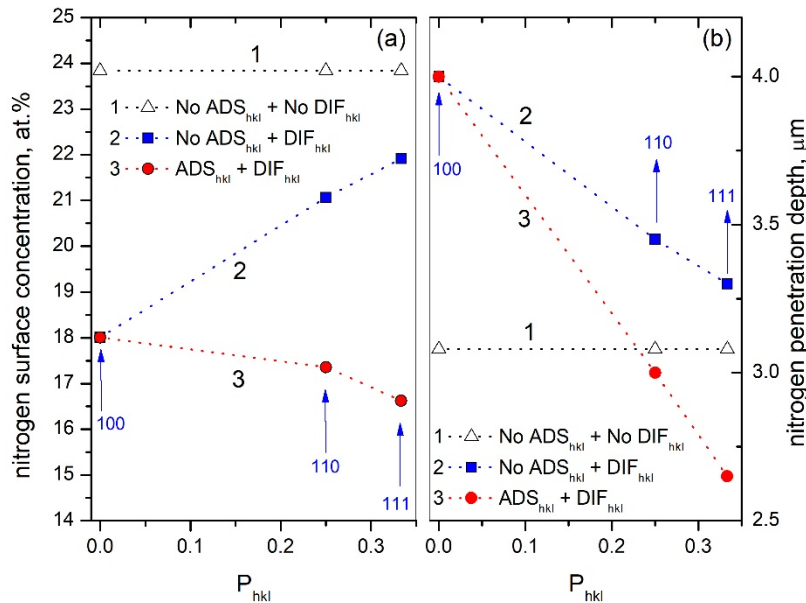


Figure 3. Dependencies of nitrogen surface concentration (a) and penetration depth (b) on parameter P_{hkl} calculated for three different cases: (1) isotropic surface processes and isotropic diffusion (No ADS_{hkl} + No DIF_{hkl}), (2) isotropic surface processes and anisotropic diffusion (No ADS_{hkl} + DIF_{hkl}), and (3) anisotropic surface processes and anisotropic diffusion (ADS_{hkl} + DIF_{hkl}).

To understand the role of anisotropic stress-assisted nitrogen and hydrogen diffusion and anisotropic effects on the steel surface on nitrogen transport, additional analysis was carried out. First, the simulation was performed using a model based on Equations (7) and (8) with an isotropic $X_{stress(hkl)}$ term and with an isotropic adsorption term $\Phi_{0\ int-hkl}$ (i.e., the values of $X_{stress(hkl)}$ and A_{hkl} were kept constant for all crystallographic orientations, No ADS_{hkl} + No DIF_{hkl} model). Second, calculations

were performed with anisotropic $X_{stress(hkl)}$ and $\Phi_{0\ int-hkl}$ terms ($ADS_{hkl} + DIF_{hkl}$ model). The results of these calculations are shown in Figure 4. Generally, the steel surfaces exhibit an oxide coverage before the nitriding, which depends on the pre-history of the steel sample. During nitriding, the oxygen content of the surface is reduced due to the hydrogen etching mechanism [33,35]. Thus, as the initial condition for calculations, the natural oxide layer of 0.5 μm thickness was taken. As can be seen in Figure 4, the shape of the oxygen concentration profiles is determined by the oxygen diffusion into the steel bulk and towards the steel surface, where it is removed by the hydrogen assistance. By comparing the nitrogen and hydrogen profiles shown in Figure 4, it was observed that coupled analysis with anisotropic effects showed a higher level of nitrogen penetration as compared to that without anisotropic effects. This clearly demonstrates that the nitrogen diffusion is enhanced by the anisotropic stress-assisted hydrogen diffusion and anisotropic effects on the surface due to interaction with $\text{N}_2\text{-H}_2$ plasma. Thus, it is important to study the kinetics of the surface processes.

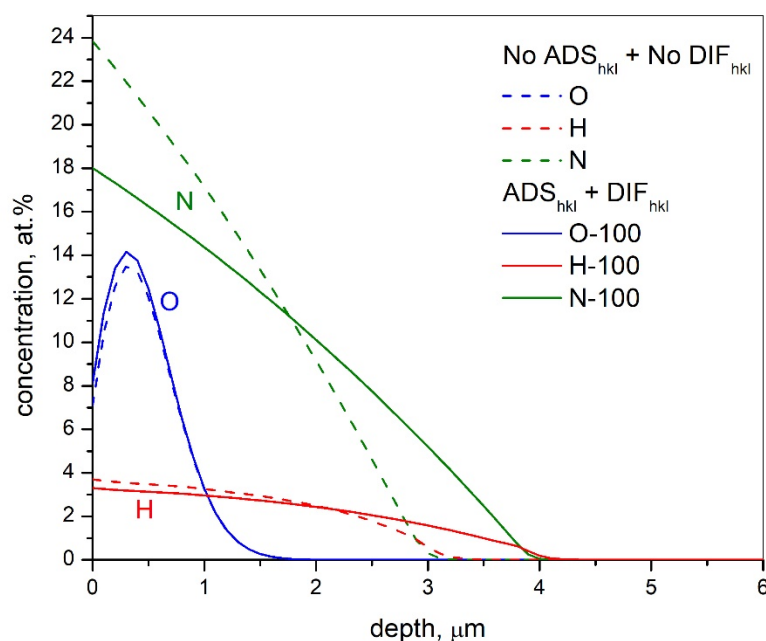


Figure 4. Depth profiles of nitrogen (N), hydrogen (H) and oxygen (O) calculated for two different cases: (1) isotropic (No ADS_{hkl} + No DIF_{hkl}) and (2) anisotropic (ADS_{hkl} + DIF_{hkl}) surface processes and diffusion.

As mentioned above, all the steps of adsorption, desorption and surface reaction processes occurring on the steel surface due to interaction with $\text{N}_2\text{-H}_2$ plasma are shown schematically in Figure 1. The kinetics of the mentioned processes were analyzed, and it was found that the main impacts on nitrogen transport are from the nitrogen/hydrogen adsorption processes and water molecule formation and subsequent desorption. The formation and desorption of water molecules causes oxygen elimination, i.e., a chemical etching of the adsorbed oxygen by hydrogen. Thus, the values of the corresponding kinetic parameters α_H , α_N and R_{H_2O} are important for the transport of nitrogen as well as for the dynamic surface concentration change. Those parameters are constants at given experimental conditions but can be varied by changing the experimental conditions, e.g., temperature or the energy of ions arriving from plasma [42]. The influences of these parameters on nitrogen penetration depth and surface concentration are shown in Figures 5–8. As can be seen in Figures 5–7, with increases in the hydrogen sticking coefficient, α_H , and water molecule formation reaction rate, constant, R_{H_2O} , the process of removing oxygen from the steel surface is enhanced and reaches a maximum. As a result, the amount of adsorbed and diffused nitrogen increases. Moreover, with a further increase in the hydrogen sticking coefficient, α_H , the surface concentration of nitrogen and nitrogen penetration depth decrease (Figure 6). It can be explained by the fact that more adsorption sites are occupied by hydrogen

and, as a result, the amount of adsorbed nitrogen decreases; consequently, the surface concentration and the penetration depth of nitrogen decrease. The dependencies of the nitrogen surface concentration and penetration depth on the nitrogen sticking coefficient, α_N , are presented in Figure 8. The nitrogen surface concentration and penetration depth increase and approach steady state values.

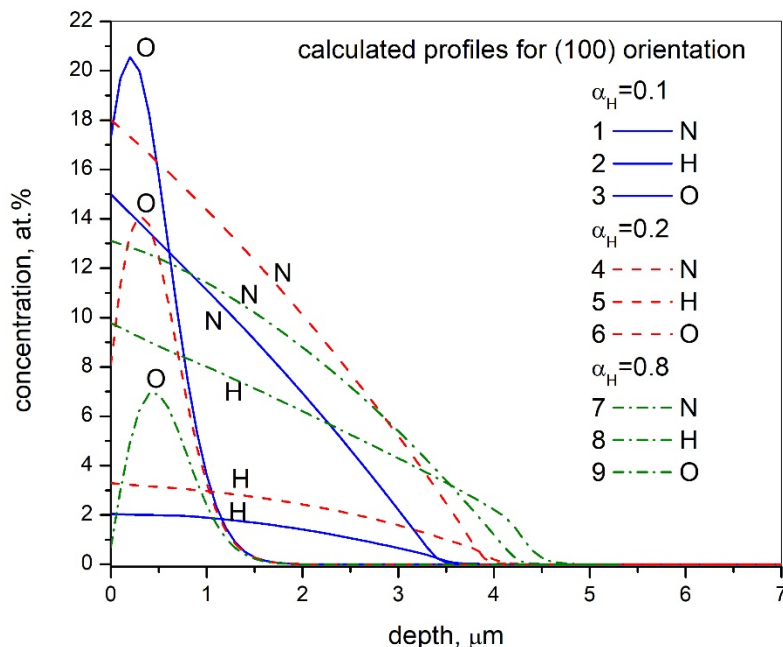


Figure 5. Depth profiles of nitrogen N, hydrogen H and oxygen O calculated at different values of parameter α_H (hydrogen adsorption sticking coefficient).

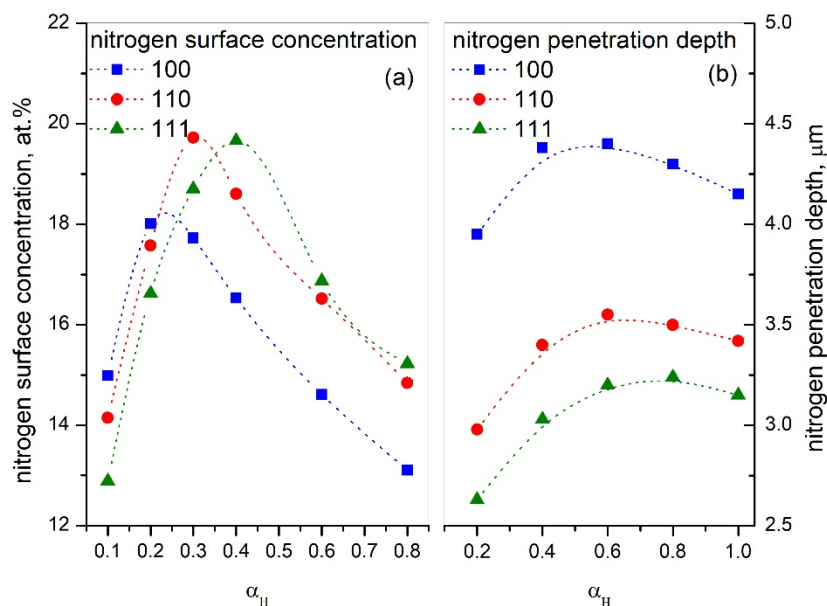


Figure 6. Nitrogen surface concentration (a) and nitrogen penetration depth (b) as functions of parameter α_H for different crystallite orientations.

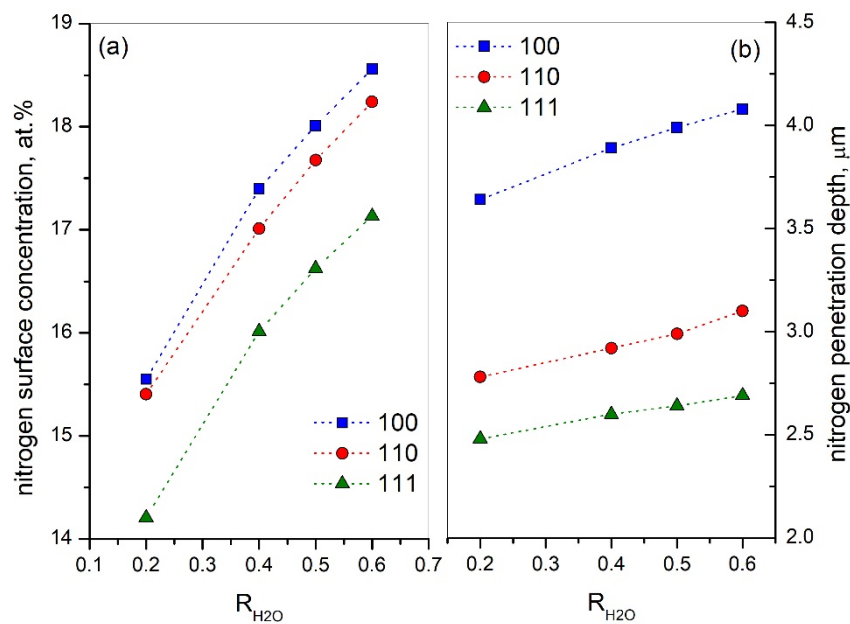


Figure 7. Nitrogen surface concentration (a) and nitrogen penetration depth (b) as functions of parameter R_{H_2O} (reaction rate of water molecule formation) for different crystallite orientations.

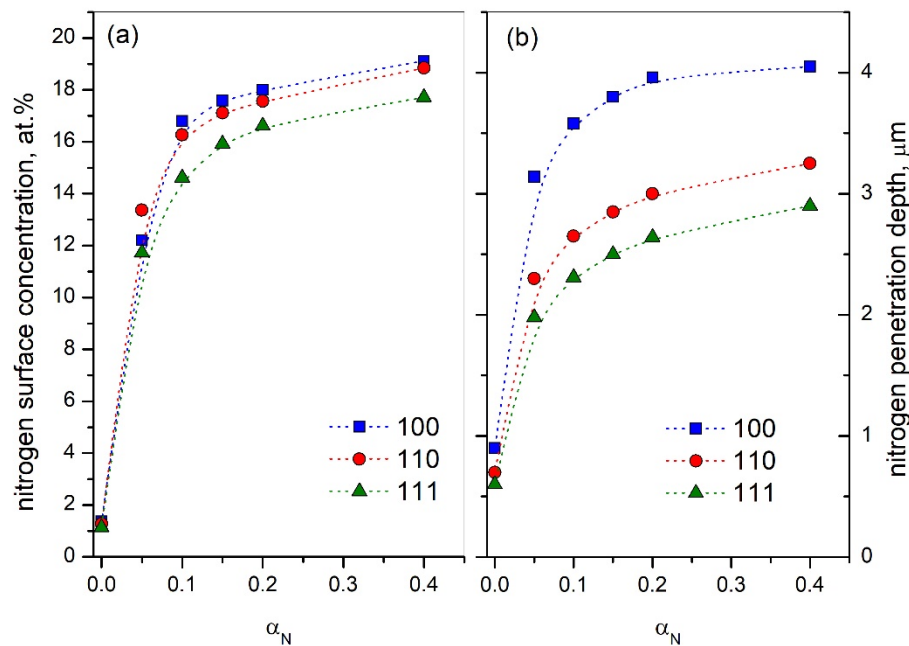


Figure 8. Nitrogen surface concentration (a) and nitrogen penetration depth (b) as functions of parameter α_N (nitrogen adsorption sticking coefficient) for different crystallite orientation.

In this study, it is shown that the anisotropic nature of lattice stresses influences the different penetration of nitrogen and hydrogen in the differently orientated grains. The grain orientation-dependent penetration of nitrogen and hydrogen is also influenced by the anisotropic nature of the processes on the surface such as adsorption and heterogeneous chemical reactions. The most important aspect is that the inclusion of the anisotropy of the surface processes into the model explains the experimental observations, i.e., that both the penetration depth and the surface concentration of nitrogen in ASS increase in the order $(100) > (110) > (111)$. The model also explains the role and influence of hydrogen in the plasma nitriding process. Hydrogen enhances nitrogen diffusion by reducing the diffusion barrier formed by the oxygen adsorbed on the steel surface during the

nitriding process (oxygen is a common contamination element in plasma chambers, directly affecting the nitriding process) and natural oxide, whose thickness depends on the pre-history of the sample. Hydrogen also influences the diffusion of nitrogen, because it creates additional lattice stresses and enhances the process of stress-induced diffusion. There is a mutual effect; hydrogen increases the diffusion of nitrogen, and conversely, nitrogen increases the diffusion of hydrogen. The proposed model can be used to optimize the nitriding process for ASS and control the morphology of the nitride layers when there is a dynamic change of atmosphere.

4. Conclusions

1. The nitrogen concentration evolution during expanded austenite formation is anisotropic due to the effects of the anisotropic stress gradient (taking into account the elastic anisotropy of ASS) and anisotropic effects on the steel surface.
2. The anisotropic nature of adsorption, desorption and heterogeneous reactions has a significant influence on the concentration evolution profiles and penetration depth of nitrogen and hydrogen.
3. The reaction rate of water molecule formation on the surface and adsorption rates of hydrogen and nitrogen are the main parameters determining the depth profile of nitrogen and its penetration depth during the nitriding of austenitic stainless steel in nitrogen/hydrogen plasma.
4. The variation of the hydrogen adsorption rate influences the nitrogen surface concentration and penetration depth non-monotonously. Both functions pass through the maxima, and it means that the optimal adsorption rate of hydrogen exists where the nitrogen depth penetration is the highest.

Author Contributions: Conceptualization, T.M. and A.G.; methodology, A.G.; software, T.M.; validation, T.M. and A.G.; formal analysis, T.M. and A.G.; investigation, T.M. and A.G.; resources, T.M. and A.G.; data curation, T.M. and A.G.; writing—original draft preparation, T.M.; writing—review and editing, A.G.; visualization, T.M.; supervision, A.G.; project administration, A.G.; funding acquisition, T.M. and A.G. All authors have read and agreed to the published version of the manuscript.

Funding: This research was funded by RESEACH COUNCIL OF LITHUANIA, grant number MIP-17103 (Reg. Nr. P-MIP-17-258).

Conflicts of Interest: The authors declare no conflict of interest.

References

1. Menthe, E.; Rie, K.T. Further investigation of the structure and properties of austenitic stainless steel after plasma nitriding. *Surf. Coat. Technol.* **1999**, *116*, 199–204. [[CrossRef](#)]
2. Menthe, E.; Rie, K.T.; Schultze, J.W.; Simson, S. Structure and properties of plasma-nitrided stainless steel. *Surf. Coat. Technol.* **1995**, *74*, 412. [[CrossRef](#)]
3. Ozturk, O.; Williamson, D.L. Phase and composition depth distribution analyses of low energy, high flux N implanted stainless steel. *J. Appl. Phys.* **1995**, *77*, 3839–3850. [[CrossRef](#)]
4. Dahm, K.L.; Dearnley, P.A. On the nature, properties and wear response of s-phase (nitrogen-alloyed stainless steel) coatings on AISI 316L. *Proc. Inst. Mech. Eng. Part L J. Mater. Des. Appl.* **2000**, *214*, 181–198. [[CrossRef](#)]
5. Sun, Y.; Li, X.Y.; Bell, T. X-ray diffraction characterisation of low temperature plasma nitrided austenitic stainless steels. *J. Mater. Sci.* **1999**, *34*, 4793–4802. [[CrossRef](#)]
6. Mingolo, N.; Tschiptschin, A.P.; Pinedo, C.E. On the formation of expanded austenite during plasma nitriding of an AISI 316L austenitic stainless steel. *Surf. Coat. Technol.* **2006**, *201*, 4215–4218. [[CrossRef](#)]
7. Mandl, S.; Rauschenbach, B. Nitrogen diffusion in austenitic stainless steel and the formation of expanded austenite. *Defects Diffus. Forum* **2001**, *188*, 125. [[CrossRef](#)]
8. Wu, D.; Kahn, H.; Dalton, J.C.; Michal, G.M.; Ernst, F.; Heuer, A.H. Orientation dependence of nitrogen supersaturation in austenitic stainless steel during low-temperature gas-phase nitriding. *Acta Mater.* **2014**, *79*, 339. [[CrossRef](#)]
9. Fewell, M.P.; Mitchell, D.R.G.; Priest, J.M.; Short, K.T.; Collins, G.A. The nature of expanded austenite. *Surf. Coat. Technol.* **2000**, *131*, 300–306. [[CrossRef](#)]

10. Keddou, M.; Marcos, G.; Thiriet, T.; Czerwicz, T.; Michel, H. Microstructural characterization of the expanded austenite formed on the plasma nitrided AISI 316 L steel. *Matériaux Tech.* **2013**, *101*, 204. [[CrossRef](#)]
11. Somers, M.A.J.; Kücükyildiz, Ö.C.; Ormstrup, C.A.; Alimadadi, H.; Hattel, J.H.; Christiansen, T.L.; Winther, G. Residual stress in expanded austenite on stainless steel; origin, measurement, and prediction. *Mater. Perform. Charact.* **2018**, *7*, 693–716. [[CrossRef](#)]
12. Christiansen, T.L.; Hummelshøj, T.S.; Somers, M.A.J. Expanded austenite, crystallography and residual stress. *Surf. Eng.* **2010**, *26*, 242–247. [[CrossRef](#)]
13. Riviere, J.P.; Pichon, L.; Drouet, M.; Poquillon, D.; Galdikas, A. Silicon based coatings deposited by dynamic ion mixing for oxidation protection of a Ti6242 alloy. *Surf. Coat. Technol.* **2007**, *201*, 8343–8347. [[CrossRef](#)]
14. Picard, S.; Memet, J.B.; Sabot, R.; Grosseau-Poussard, J.L.; Rivière, J.P.; Meilland, R. Corrosion behaviour, microhardness and surface characterisation of low energy, high current ion implanted austenitic stainless steel. *Mater. Sci. Eng. A* **2001**, *303*, 163–172. [[CrossRef](#)]
15. Borgioli, F. From austenitic stainless steel to expanded austenite-S phase: Formation, characteristics and properties of an elusive metastable phase. *Metals* **2020**, *10*, 187. [[CrossRef](#)]
16. Martinavičius, A.; Abrasonis, G.; Möller, W. Influence of crystal orientation and ion bombardment on the nitrogen diffusivity in single-crystalline austenitic stainless steel. *J. Appl. Phys.* **2011**, *110*, 075907. [[CrossRef](#)]
17. Akhlaghi, M.; Jung, M.; Meka, S.R.; Fonović, M.; Leineweber, A.; Mittemeijer, E.J. Dependence of the nitriding rate of ferritic and austenitic substrates on the crystallographic orientation of surface grains; gaseous nitriding of Fe-Cr and Ni-Ti alloys. *Philos. Mag.* **2015**, *95*, 4143–4160. [[CrossRef](#)]
18. Menéndez, E.; Templier, C.; Garcia-Ramirez, P.; Santiso, J.; Vantomme, A.; Temst, K.; Nogués, J. Magnetic properties of single crystalline expanded austenite obtained by plasma nitriding of austenitic stainless steel single crystals. *ACS Appl. Mater. Interfaces* **2013**, *5*, 10118–10126. [[CrossRef](#)]
19. Fewell, M.P.; Priest, J.M. High-order diffractometry of expanded austenite using synchrotron radiation. *Surf. Coat. Technol.* **2008**, *202*, 802–1815. [[CrossRef](#)]
20. He, H.; Zou, J.X.; Dong, C.; Czerwicz, T.; Michel, H. Stress induced anisotropic diffusion during plasma-assisted nitriding of a Ni-based alloy. *Mater. Sci. Forum* **2005**, *475*, 3669–3672. [[CrossRef](#)]
21. Kahn, H.; Michal, G.M.; Ernst, F.; Heuer, A.H. Poisson effects on X-ray diffraction patterns in low-temperature-carburized austenitic stainless steel. *Metall. Mater. Trans. A* **2009**, *40*, 1799–1804. [[CrossRef](#)]
22. Mändl, S.; Rauschenbach, B. Anisotropic strain in nitrided austenitic stainless steel. *J. Appl. Phys.* **2000**, *88*, 3323–3329. [[CrossRef](#)]
23. Moskaliuviene, T.; Galdikas, A. Stress induced nitrogen diffusion in nitrided austenitic stainless steel. *Mater. Sci.* **2011**, *17*, 11–15. [[CrossRef](#)]
24. Galdikas, A.; Moskaliuviene, T. Swelling effect on stress induced and concentration dependent diffusion of nitrogen in plasma nitrided austenitic stainless steel. *Comput. Mater. Sci.* **2013**, *72*, 140–145. [[CrossRef](#)]
25. Moskaliuviene, T.; Galdikas, A. The effect of hydrogen on plasma nitriding of austenitic stainless steel: Kinetic modeling. *Metall. Mater. Trans. A* **2015**, *46*, 5588–5595. [[CrossRef](#)]
26. Moskaliuviene, T.; Galdikas, A. Kinetic model of anisotropic stress assisted diffusion of nitrogen in nitrided austenitic stainless steel. *Surf. Coat. Technol.* **2019**, *366*, 277–285. [[CrossRef](#)]
27. Galdikas, A.; Moskaliuviene, T. Stress induced nitrogen diffusion during nitriding of austenitic stainless steel. *Comput. Mater. Sci.* **2010**, *50*, 796–799. [[CrossRef](#)]
28. Reuss, A. Berechnung der Fließgrenze von Mischkristallen auf Grund der Plastizitätsbedingung für Einkristalle. *ZAMM-Zeitschrift Für Angewandte Mathematik Und Mechanik.* **1929**, *9*, 49–58. [[CrossRef](#)]
29. Zoltowski, P. Effects of self-induced mechanical stress in hydrogen sorption by metals, by EIS. *Electrochim. Acta* **1999**, *44*, 4415. [[CrossRef](#)]
30. Baranowski, B. *Advances in Thermodynamics: Flow, Diffusion and Rate Processes*; Saniutycz, S., Salamon, P., Eds.; Taylor and Francis: New York, NY, USA, 1992; pp. 168–199.
31. Zhang, L.; Barrett, R.; Cloetens, P.; Detlefs, C.; Rio, M.S. Anisotropic elasticity of silicon and its application to the modelling of X-ray optics. *J. Synchrotron Radiat.* **2014**, *21*, 507–517. [[CrossRef](#)]
32. He, H.; Czerwicz, T.; Dong, C.; Michel, H. Effect of grain orientation on the nitriding rate of a nickel base alloy studied by electron backscatter diffraction. *Surf. Coat. Technol.* **2003**, *163–164*, 331–338. [[CrossRef](#)]
33. Figueroa, C.A.; Wisnivesky, D.; Alvarez, F. Effect of hydrogen and oxygen on stainless steel nitriding. *J. Appl. Phys.* **2002**, *92*, 764–770. [[CrossRef](#)]

34. Wang, L.; Xu, X.; Yu, Z.; Hei, Z. Low pressure plasma arc source ion nitriding of austenitic stainless steel. *Surf. Coat. Technol.* **2000**, *124*, 93–96. [[CrossRef](#)]
35. Figueroa, C.A.; Weber, S.; Czerwicz, T.; Alvarez, F. Oxygen, hydrogen, and deuterium effects on plasma nitriding of metal alloys. *Scr. Mater.* **2006**, *54*, 1335–1338. [[CrossRef](#)]
36. Moskalioviene, T.; Galdikas, A. Mechanisms of the hydrogen influence on the diffusivity of nitrogen during plasma nitriding austenitic stainless steel. *Metall. Mater. Trans. A* **2019**, *50*, 1021–1032. [[CrossRef](#)]
37. Zangwill, A. *Physics at Surfaces*; Cambridge University Press: New York, NY, USA, 1988.
38. Einstein, T.L. Equilibrium Shape of Crystals. In *Handbook of Crystal Growth: Fundamentals*; Nishinaga, T., Ed.; Elsevier: Amsterdam, The Netherlands, 2014; Volume 1, pp. 215–264. [[CrossRef](#)]
39. Yu, Z.; Flodstrom, A. Orientation of (1×1)-surface free energies of crystals. *Surf. Sci.* **1998**, *401*, 236–247. [[CrossRef](#)]
40. Jian-Min, Z.; Fei, M.; Ke-Wei, X. Calculation of the surface energy of fcc metals with modified embedded-atom method. *Chin. Phys.* **2004**, *13*, 1082–1090. [[CrossRef](#)]
41. Gressmann, T.; Wohlschlogel, M.; Shang, S.; Welzel, U.; Leineweber, A.; Mittemeijer, E.J.; Liu, Z.K. Elastic anisotropy of γ' -Fe₄N and elastic grain interaction in γ' -Fe₄N_{1-y} layers on α -Fe: First-principles calculations and diffraction stress measurements. *Acta Mater.* **2007**, *55*, 5833–5843. [[CrossRef](#)]
42. Galdikas, A.; Pranevičius, L. Surface composition changes of ternary alloys in the nonsteady state regime of preferential sputtering. *Nucl. Instrum. Methods Phys. Res. Sect. B Beam Interact. Mater. At.* **2000**, *164*, 868–871. [[CrossRef](#)]



© 2020 by the authors. Licensee MDPI, Basel, Switzerland. This article is an open access article distributed under the terms and conditions of the Creative Commons Attribution (CC BY) license (<http://creativecommons.org/licenses/by/4.0/>).